

## Original Research Article

# An investigation on sintering behavior of nanostructured Cu-10, 20 wt. % Ni alloy powders

Hurieh Mohammadzadeh<sup>a,\*</sup> , Roya Roohibakhsh<sup>b</sup>, Hamid Reza Rezaie<sup>b</sup>

<sup>a</sup> Faculty of Engineering, Urmia University, Urmia, Iran

<sup>b</sup> School of Metallurgical and Materials Engineering, Iran University of Science and Technology (IUST), Tehran, Iran

### ARTICLE INFORMATION

Received: 16 September 2020  
Received in revised: 23 October 2020  
Accepted: 12 December 2020  
Available online: 26 January 2021

DOI: 10.26655/AJNANOMAT.2021.2.1

### KEYWORDS

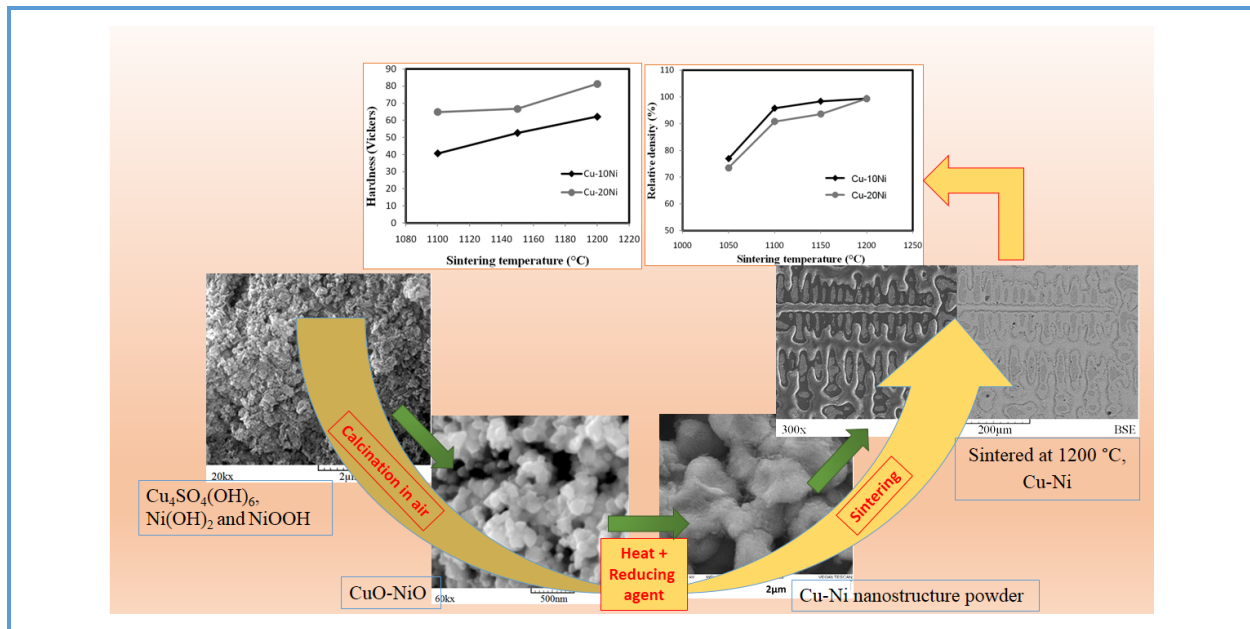
Cu-Ni nano-structure powder  
Chemical precipitation  
Powder metallurgy  
Sintering Cu-Ni composite powder

### ABSTRACT

In this research study, nano-composite powder of Cu-Ni was synthesized from precursor salts of copper and nickel sulfates through chemical co-precipitation to yield the final product of Cu-10 and 20 wt. % Ni. The chemical co-precipitation was followed by two steps of thermal and thermochemical treatments; calcination and reduction, respectively. The compounds of  $\text{Cu}_4\text{SO}_4(\text{OH})_6$ ,  $\text{Ni}(\text{OH})_2$  and  $\text{NiOOH}$  were identified as green precipitation which was then calcined at 850 °C for 1 h to CuO-NiO. The reduction process, by hydrogen at 700 °C for 1 h, led to Cu-Ni nanostructure powder with crystallite size of 18-33 nm. This powder was sintered at different temperatures of 1050-1200 °C for 2 h. The microstructure of synthesized powders and sintered products were evaluated using the scanning electron microscope (SEM). The value of microhardness and density, and porosity content of the sintered samples were measured. For all sintering temperatures the lowest porosity and the highest value of density were observed for Cu-10% Ni. At the sintering temperature of 1200 °C, the relative density for both samples was similar, 99.4%. Maximum value of hardness, 81.22 Vickers, was obtained for Cu-20% Ni chemical composition which was sintered at 1200 °C. Energy Dispersive Spectroscopy (EDS) which was employed for elemental mapping revealed the elemental segregation of Cu and Ni towards inter-dendrite and dendrites regions, respectively, for the samples sintered at 1200 °C.

© 2021 by SPC (Sami Publishing Company), Asian Journal of Nanoscience and Materials, Reproduction is permitted for noncommercial purposes.

## Graphical Abstract



## Introduction

The technology of manipulating metal powders into the forms of specific shapes, known as powder metallurgy (PM), has made it feasible to produce new strong alloys with perfect control on microstructure and other properties. PM is a successful method in producing final components with the least impurities and unwanted elements. High reactivity of powder and specially nano-powder materials makes low temperature PM more efficient in producing bulk product with the lowest unwanted defects. Conventional casting methods which suffer of such defects could be successfully replaced with PM benefiting advantages of high accuracy, minimum final machining requirements and no defects of impurities and shrinkage, and also the advantage of the low temperature processing [1–3].

Copper powder production is interested by scientists and industries due to outstanding properties such as high electrical conductivity,

relatively higher melting point, excellent solderability, low electrochemical migration and low material cost [4]. The relative weak oxidation resistance of ultrafine copper powders can be improved by composing with other metals, such as Ni, Al, Mg, and Ag in bimetallic or alloy forms. Bimetallic copper-nickel, as a special combination with an extensive industrial use, does not oxidize at ambient temperature [4–6]. Moreover, the presence of Ni nano-particles in the components can improve the magnetic properties from diamagnetic to ferromagnetic [7, 8]. In addition, Ni in Cu–Ni alloys can enhance tensile strength, hardness and corrosion resistance [9].

High corrosion resistance of this alloy makes it a good candidate for components in constructing condensers, heat exchangers, piping in saltwater, pumps, boats, ship bodies and also for aggressive environments such as acidic and basic solutions containing alkaline compounds and petroleum materials. In some cases, these alloys are used in plane blades and

cranks [10–13]. Although Cu–Ni alloys are commonly produced through mixing molten metals of Cu and Ni through casting, PM benefits sintering under specific conditions which can result in desired alloy compounds.

Sintering is a dominant step in PM which affects strongly the final properties such as strength, hardness, corrosion and conductivity. Although bonding of particles occurs at the first step by solid state surface diffusion, the major condensation happens when liquid forms during a liquid phase sintering (LPS), which activates the mechanisms of liquid spreading and rearrangement by capillary forces. These mechanisms act to pull particles together and cause rearrangement and densification of the compact [14]. It is expected that the particle size of the participating powders influence sintering mechanisms, particularly when the diameter is less than 50 nm. The complexity of contributions of large surface area for nano particles through compaction and sintering, due to associated high level of energy, would alter the sinterability and microstructure of the product, especially when mutual solubility of components are involved [15, 16]. To enlighten the dark sides of microstructure evolutions during sintering nano powder of Cu–Ni, in the present study, a range of temperatures was employed to investigate the effect of liquid flow in rearrangement and connection of particles. Therefore, the Cu–Ni nano-sized powder, which was synthesized through chemical precipitation, was solidified. The consolidation behavior was studied thoroughly based on final density and mechanical and microstructural properties and finally was compared with literature and effect of particle size was discussed.

## Experimental

### *Materials and sample preparation*

Copper sulfate ( $\text{CuSO}_4 \cdot 3\text{H}_2\text{O}$ , >99%, China), nickel sulfate ( $\text{NiSO}_4 \cdot 3\text{H}_2\text{O}$ , >99%, China) and sodium hydroxide ( $\text{NaOH}$ , >99%, Merck, Germany) were used as precursors. Copper and nickel sulfate solutions were prepared separately by dissolving the corresponding salts in distilled water, followed by mixing the solutions together. The ratio of Ni and W salts was based on the stoichiometric proportions to produce the final products of 10 and 20 wt. % Ni in Cu. The mixed solution was heated at about 70 °C and stirred simultaneously. pH was adjusted to be 9 by gradually adding of sodium hydroxide. After 5 h at 70 °C, the resulted suspension was aged for 20 h at room temperature. The precipitates were then washed with distilled water for 10–12 times and dried at 100 °C for 4 h. The green precipitates were calcined in an electrical furnace for 1 h at 850 °C, based on Simultaneous Thermal Analysis (STA) results. The calcined powders were reduced in hydrogen for 1 h with a heating rate of 10 °C/min at 700 °C which resulted in Cu–Ni nanostructure powders. This product was then pressed under a uniaxial pressure of 200 MPa in a die with 10 mm diameter. Sintering of the compacts was performed in a tube-type electrical furnace under hydrogen with a heating rate of 10 °C/min up to 1050–1200 °C for 2 h.

### *Characterization*

Initial precipitates, and calcined and reduced powders were all characterized by X-ray diffractometry (XRD) (JEOL, JDX-8030), Cu-K $\alpha$ ,  $\lambda=1.5406\text{\AA}$ , to identify the resulted phases. Based on XRD results, the crystallite size of products was calculated through measuring the broadening of main diffraction peaks, using Scherrer equation. To determine the appropriate calcination temperature, the dried precipitates were subjected to STA, providing a simultaneous application of Thermogravimetry

(TGA) and Differential Scanning Calorimetry (DSC), Shimadzu (model: DTA 50&TGA-50), by heating the precipitated sample up to 1100 °C with a heating rate of 10 °C/min in air. The microstructure of the synthesized and sintered powders was investigated using the scanning electron microscope (SEM, JEOL JSM-6360). The image analysis software of Clemex was employed to determine the particle size of SEM images. EDS elemental map, linear, and point scan analysis of elemental distribution were conducted using the energy dispersive X-ray analysis (EDX) to investigate the distribution of Ni and Cu, and also the composition of product at different points of sintered samples. The density of samples was measured by Archimedes method. The hardness was measured by a micro-hardness tester (BOHLER, model: MXT-al) at four different points for each sample; the average value was reported.

## Results and Discussion

### *Synthesis of Cu- 10, 20% Ni powder (chemical precipitation, calcination and reduction)*

To co-precipitate the compounds from the pH was adjusted to 9 which resulted to the precipitation of brochantite ( $\text{CuSO}_4 \cdot 3\text{Cu}(\text{OH})_2$  or  $\text{Cu}_4(\text{OH})_6\text{SO}_4$ ) and nickel hydroxide ( $\text{NiOOH}$  and  $\text{Ni}(\text{OH})_2$ ) which were detected by XRD analysis of dried samples for both 10 and 20% Ni (Figure 1a, along with the structure of the main components). The study of diffraction pattern of dried samples confirmed the trace of Ni content on the resulted phases. By changing the chemical composition from 10% of Ni to 20%, the peaks of nickel hydroxides were strengthened, while brochantite peaks got weaker. This shows the participation of Ni in the form of consequent hydroxide phases. The average crystallite size of precipitates for Cu-10% Ni and Cu-20% Ni samples were

determined by Scherrer equation on the main peaks to be 18.16 and 21.78 nm, respectively.

Based on STA analysis (Figure 1b), the precipitates were calcined at 850 °C for 1 h in air. STA graph showed multiple peaks in Figure 1b including an endothermic peak at 796 °C which can stem from the decomposition of sulfate and hydroxide phases to copper and nickel oxides. This peak was reported in the literature as well [17–19]. A detailed study on series of calcination of brochantite at 200 to 800 °C [20] revealed a complete calcination 750–800 °C and also Mohammadzadeh *et al.*, [21] reported  $\text{NiOOH}$  and  $\text{Ni}(\text{OH})_2$  calcination before 600 °C.

The XRD patterns of calcined products of 10 and 20% Ni are shown in Figure 1c, indicating the presence of oxide phases of copper (II) ( $\text{CuO}$ ) and nickel ( $\text{NiO}$ ). Moreover, there is a slight increase of intensity for nickel oxide peaks at higher weight percent of nickel. The particle size resulted by image analysis (Clemex software) was found to be 78 nm for the average diameter of 50 measurements on SEM images. Since larger pieces in the images were obviously agglomerates of their participants, they cannot be supposed as real representative of prime particles. Therefore, the main fine particles were dimensionally characterized. In addition, Scherrer equation was applied on main peaks of XRD pattern to determine the crystallite size. The results of 10 and 20% Ni were equal to 30.2 nm and 30.3 nm, respectively. There is a small difference between measured and calculated particle size which is normal in nano scale through the enhanced agglomeration of constituents.

Figure 2a and Figure 2b present the XRD patterns of reduced products, with different nickel contents, which were thermochemically treated under hydrogen at 700 °C for 1 h. As seen, there is overlapping for some peaks, and moreover, the location of diffract peaks for

copper slightly shifts from its location in pure copper to that of nickel, which is very close to two bimetallic components of  $\text{Ni}_{19}\text{Cu}_{81}$  and  $\text{Ni}_{21}\text{Cu}_{79}$ , given by JCPDS, files number of 47-1406 and 09-0205, respectively. Calculated

crystallite size of reduced products for samples with 10 and 20% Ni were equal to 33.5 and 30.5 nm, respectively which are similar to the oxide phases, reported earlier.

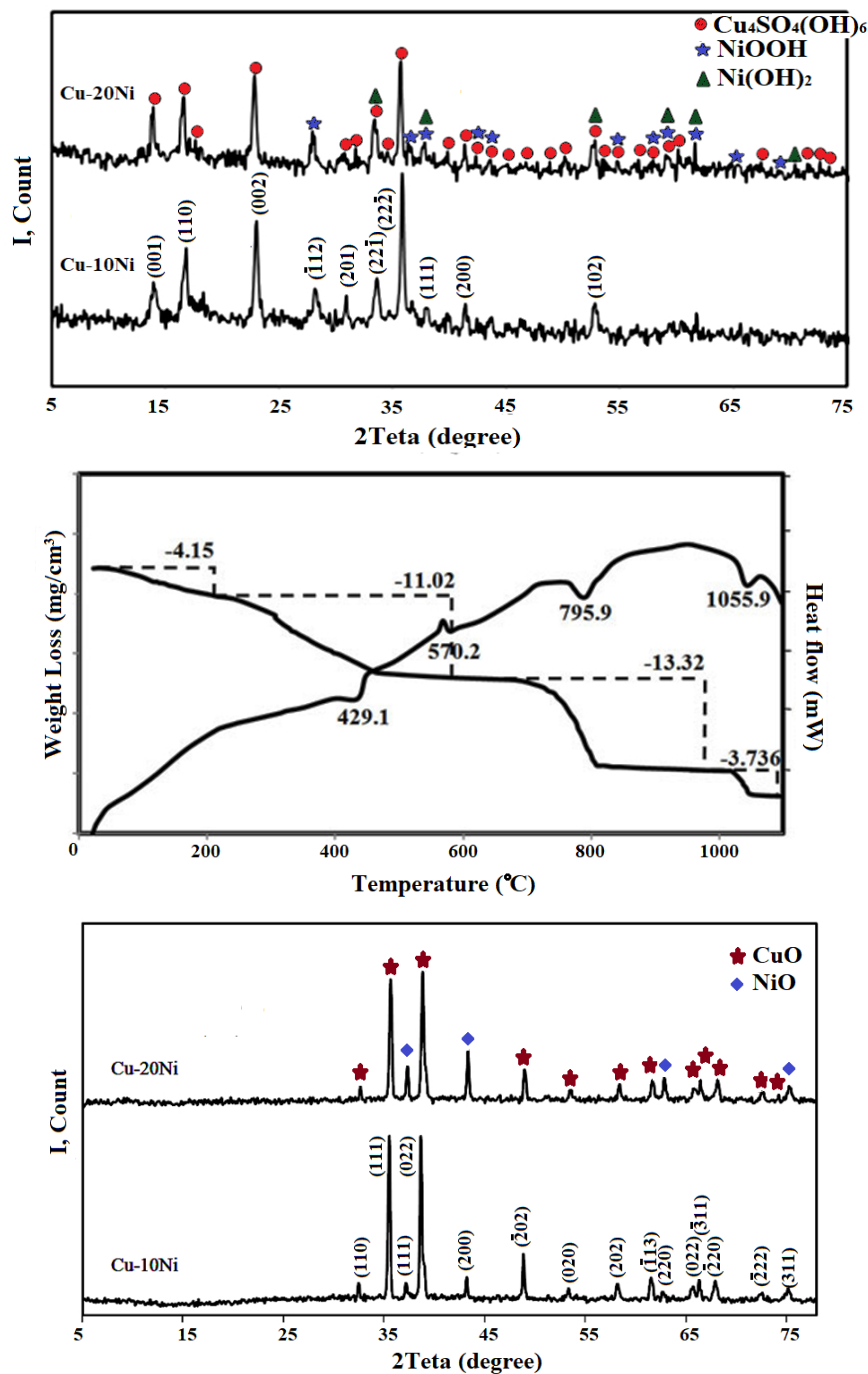


**Figure 1.** a) XRD pattern of Cu-10 and 20% Ni for as-precipitated powders, and the atomic structure of main phases, b) STA analysis of the initial precipitates heated up to 1100 °C with heating rate of 10 °C/min in air and, c) XRD pattern of Cu-10 and 20% Ni of calcined products

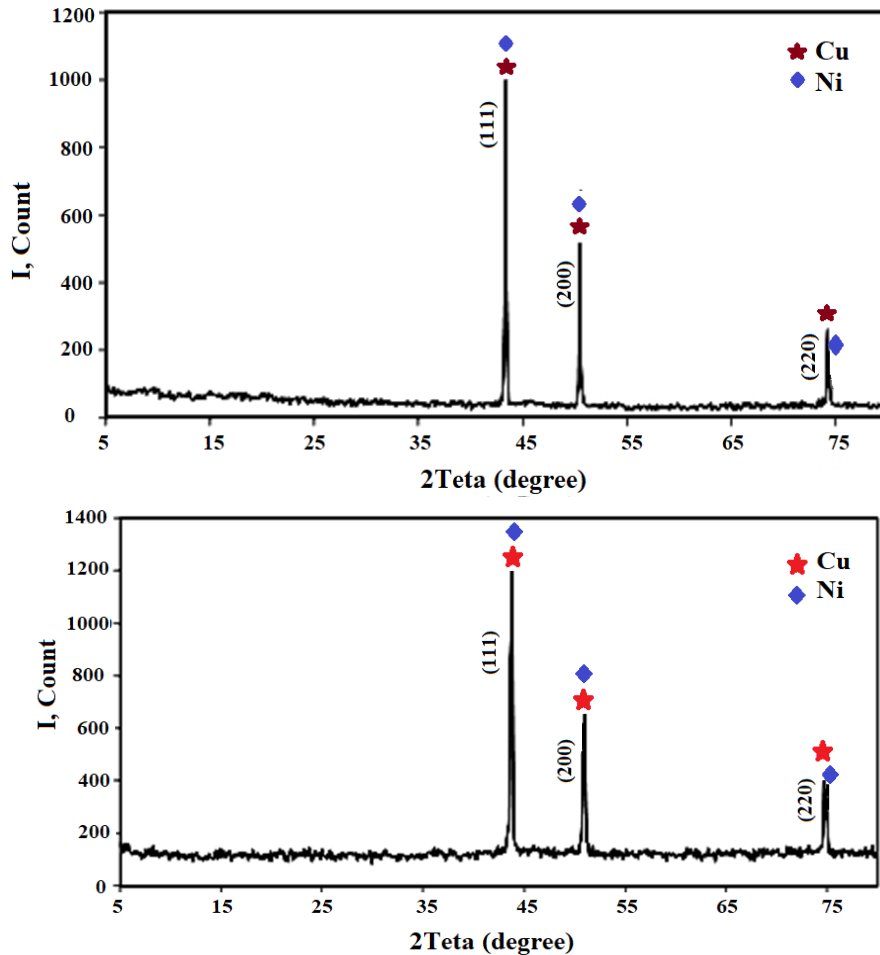


**Figure 2.** XRD patterns of reduced powder for a) 1 Cu-10% Ni and b) Cu- 20% Ni

Figure 3 illustrates the SEM micrographs of the products for three steps of precipitation, calcination, and reduction. The microstructure of initial dried precipitates for different nickel contents, Figure 3a and Figure 3b for 10% and 20% Ni, respectively, depicts agglomerated product with platelet-like or rock-like morphologies. Such accumulation of particles is more obvious at higher nickel content. This can suggest that the agglomeration was probably promoted by hydroxide phase of Ni. Moreover, the elemental distribution of Ni and Cu are presented in Figure 3c and Figure 3d, respectively, associated to the SEM image of Figure 3a for Cu-10% Ni, and accordingly elemental maps of Ni and Cu for 20% Ni of

Figure 3b are illustrated in Figure 3e and Figure 3f, respectively. As seen, uniform distribution of these elements are observable with no undesired individual aggregations of Ni or Cu.

SEM micrographs of the calcined products are depicted in Figure 4a and Figure 4b, for the samples of 10 and 20% Ni, respectively. As can be seen, the microstructure of calcined products consist of monodispersed and small quasi-spherical particles, in contrast to the agglomerated feature for dried products which can be related to the hydroxide ligands in the structure of nickel oxide and copper sulfate. This ligand was removed in the calcined product.

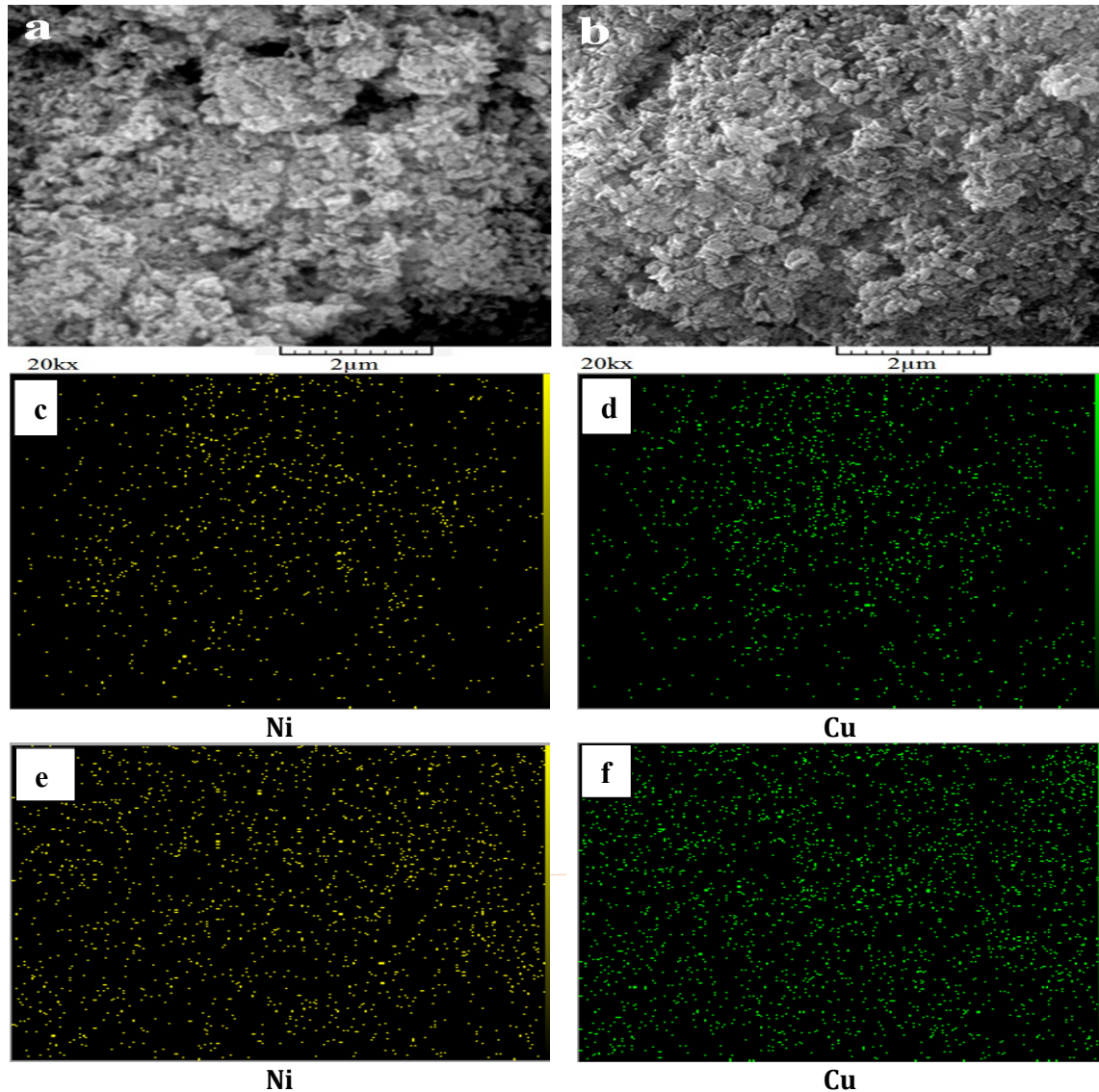


**Figure 3.** SEM micrographs of the initial precipitates for synthesis of a) Cu-10% Ni and b) Cu-20% Ni, and the elemental map of Ni and Cu for c, d) Cu-10% Ni and e, f) Cu-20% Ni

The study on the microstructure of reduced powder, 10% and 20% Ni in [Figure 4c](#) and [Figure 4d](#), respectively, revealed a serious agglomeration and obvious adhesion between particles, in contrast to the oxide state of calcined products. This makes it unsatisfied to measure a trustable particle size by Clemex Image Analyzer. It should be noted that Ni (as element) is a ferromagnetic material. The saturation magnetization of pure nickel has been measured to be 55.1 emu/g in its bulk form [22].

Refining nickel as fine nanosized particles and also mixing it with a non-magnetic material, Cu in this case, would change magnetic characteristics, in terms of coercivity and saturation magnetization respectively; for Cu-10 and 20 wt. % Ni of the current study, the saturation magnetization lowered to about 6.2 and 6.8 emu/g and the coercivity was increased from 0.7 Oe for bulk Ni to 125 and 143 Oe for 10 [23] and 20 wt. % Ni ([Figure 5](#)).

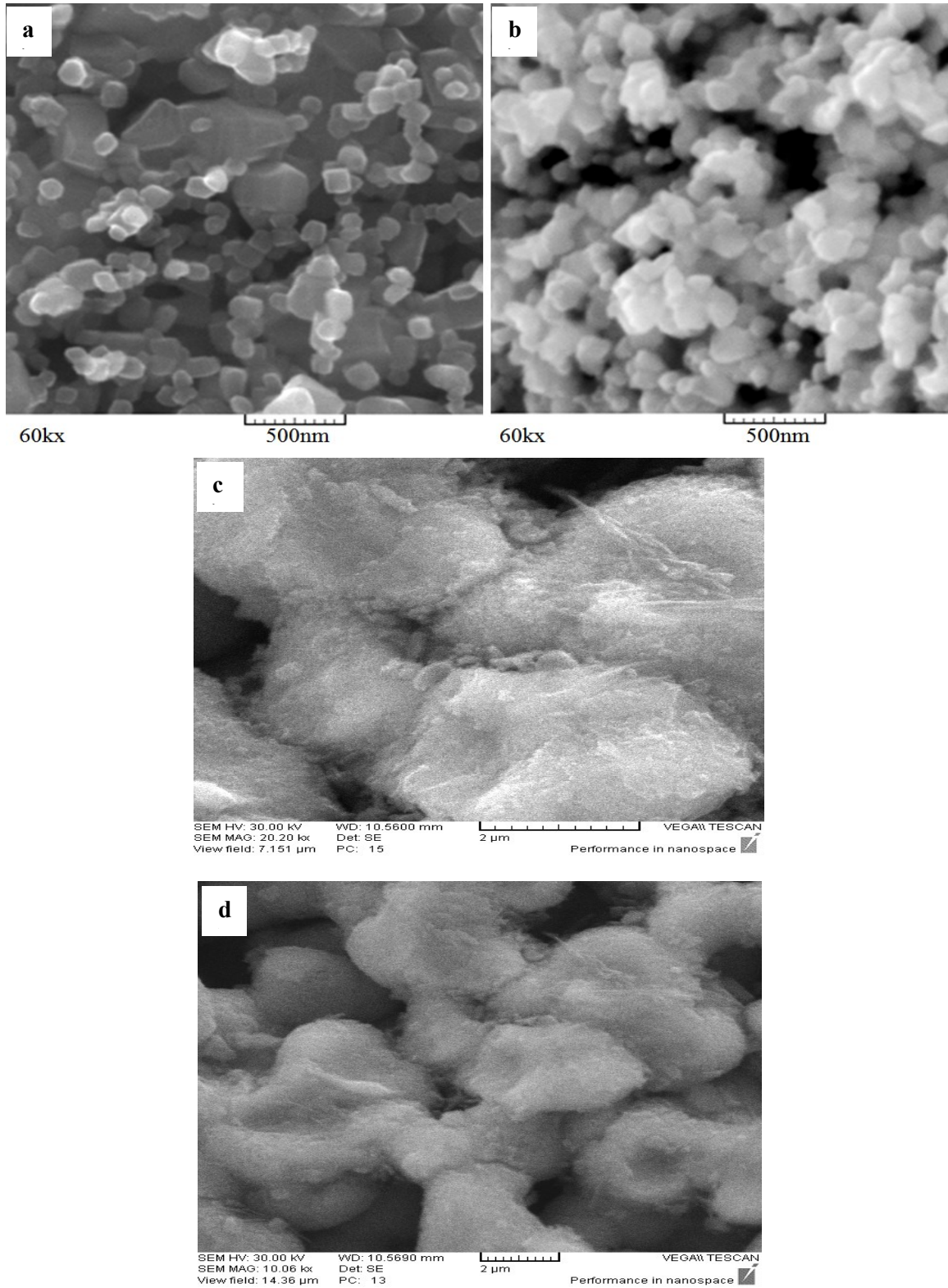


**Figure 4.** SEM micrographs of products calcined at 850 °C for a) Cu-10% Ni and b) Cu-20% Ni, and reduced powders at 700 °C in hydrogen for c) Cu-10% Ni and d) Cu-20% Ni



Later is another confirmation for particle size refinement of the products of chemical precipitation method. At particle size below micrometer ( $<1 \mu\text{m}$ ), the single domain of ferromagnetic particles needs to have spin rotation in the magnetic field instead of domain wall displacement, which results in higher required magnetic fields [24]. The composite powder produced by chemical co-precipitation benefits a nano-scaled distribution of

constitutional elements, in addition to the nano scale of particles. Nickel in its oxide form represent antiferromagnetic feature which means it is not attracted in the magnetic field and would form monodispersed particles as seen in Figure 4a and Figure 4b. Such ferromagnetic attraction between Ni particles can enhance the agglomeration in Cu-Ni reduced form which is obvious in Figure 4c and Figure 4d.

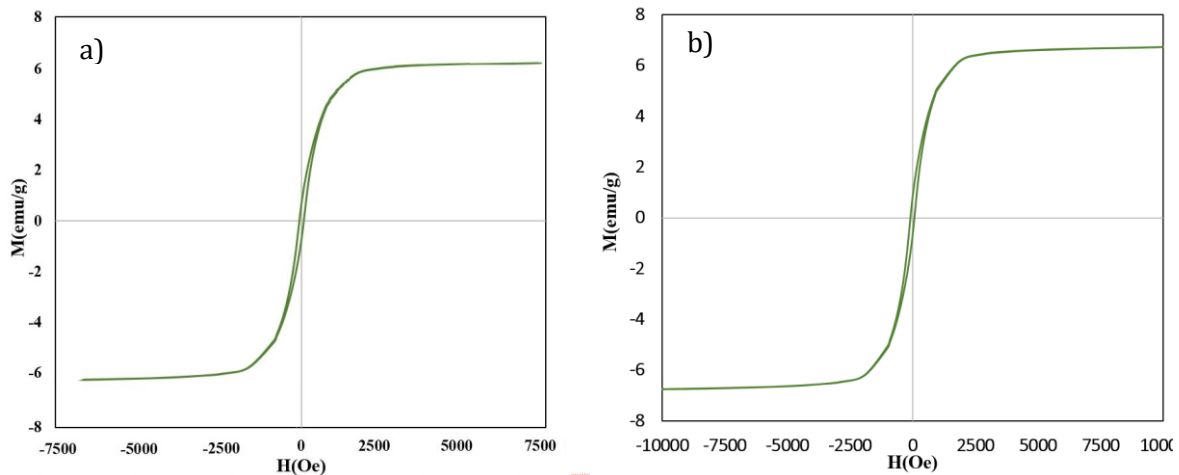


**Figure 5.** Magnetization hysteresis loop for reduced powder of a) Cu-10% Ni and b) Cu-20% Ni

### Sintering of reduced powders

Different sintering temperatures and nickel contents were studied to determine the coherent factors affecting microstructure, relative density and hardness which would help to generate optimum parameters. The relative densities of sintered samples at different temperatures, determined by Archimedes method, are presented with more details in Table 1.

Figure 6a demonstrates the curves of relative density vs. sintering temperature for different Ni % which shows improvement of density by increasing sintering temperature from 1050 to 1200 °C for both nickel contents of 10% and 20%. As seen, the relative density of samples after sintering above copper melting

point (1083 °C) began to increase significantly. By forming liquid copper at temperatures higher than melting point, LPS activates which gives rise to some efficient mechanisms of densification and condensation by creating the largest possible contact area between liquid and solid phase [25]. Above melting temperature of Cu, considerable densification was obtained (Figure 6) more possibly by liquid Cu being pulled by capillary forces into the narrow gaps between Ni solid particles, filling pores and gaps. This is confirmed by microstructural study on Figure 7 which will be discussed thoroughly later. Furthermore, liquid formation can promote the rearrangement of particles leading to more homogeneous distribution of particles in the compressed body. This is reported in previous studies on Cu-Ni system

[26–29]. Further increasing of sintering temperature can reduce viscosity of the formed liquid Cu which can affect consolidation positively, as well. Consequently, it is expected that the higher volume of liquid Cu would be responsible for good densification of the sample of Cu-10% Ni. In LPS the behavior of the liquid depends on solid-liquid surface tension, termed as wettability, which is highly affected by the mutual solubility of participants; Cu and Ni in this case. As Ni and Cu have 100% solubility, it is expected that LPS would enhance compaction considerably.

The lowest porosity and the highest value of density were obtained for the sample of Cu-10% Ni at all sintering temperatures applied in this study, except for 1200 °C at which the sample of 20% Ni showed similar relative densification. This can mean that at this temperature, possibly the promoted fluidity of Cu and wettability of liquid phase on solid particles (due to enhanced

solubility at higher temperature) have justly compensated the lower amount of liquid phase.

The variation of microhardness by sintering temperature and chemical composition of Ni content are depicted in Figure 6b. As seen the, the hardness is improved by increasing sintering temperature to 1200 °C, which was accompanied by diminishing of pores. Moreover, the results showed that Ni that possesses higher hardness in comparison to copper, has improved the hardness. Comparing Figure 6a and Figure 6b for temperature of 1200 °C that although both samples of 10 and 20% Ni showed similar, nearly full densification, but higher Ni content in the sample of Cu-20% Ni has affected the hardness positively. It has been reported by previous studies as well that the mechanical properties of copper can increase when it is composed with nickel [30–32]. The maximum value of hardness was equal to 81.22 Vickers for Cu-20% Ni, sintered at 1200 °C.

**Table 1.** Calculated relative density based on Archimedes method at different sintering temperatures for two samples of Cu-10% Ni and Cu-20 % Ni

Sample code	Sintering temperature (°C)	Apparent Porosity (%)	Water Absorption (%)	Relative Density (%)	Microhardness Hv <sub>0.1</sub>
Cu-10 % Ni	1050	9.27	1.6	76.97	35.01
Cu-20 % Ni		18.2	2.8	73.52	48.63
Cu-10 % Ni	1100	8.3	1.06	95.8	40.72
Cu-20 % Ni		16.6	2.47	90.84	65.06
Cu-10 % Ni	1150	1.3	0.149	98.39	53.07
Cu-20 % Ni		14.96	2.11	93.63	66.9
Cu-10 % Ni	1200	1.01	0.11	99.45	62.14
Cu-20 % Ni		1.09	0.12	99.4	81.22

The SEM images of the sintered samples at 1050-1150 °C under H<sub>2</sub> atmosphere are shown in Figure 7. As can be seen, at higher sintering temperature and copper content, the apparent porosity in the matrix obviously decreased by enhanced fluidity and amount of liquid copper, respectively. The liquid copper fills almost all

pores and gaps for the samples sintered at 1150 °C (Figure 7e and Figure 7f) which is above melting temperature of Cu. Sintering samples at 1050 °C, below melting point of copper, occurred in solid state, as a result there were considerable volume of pores remained unfilled (Figure 7a and Figure 7b). As solid phase of Cu-

Ni does not flow into interparticle spacing or grain boundaries, nearly full densification was not achieved at this temperature.

For the highest sintering temperature of 1200 °C, the samples with different values of Ni were etched by acidic solution in order to study the cross section microstructure (Figure 8). As seen in these images, sintering temperature of 1200 °C was high enough to result in dendritic structure, detectable in the images, which is more perceivable at higher nickel content of Figure 8c and Figure 8d.

The concentration of Cu and Ni elements in the microstructure of Cu-10% Ni, sintered at 1200 °C, was studied with more details. Accordingly, two points in dark and light areas of this sample which are labeled as A and B respectively in Figure 8a, were selected for energy dispersive spectroscopy (EDS) point analysis. The results showed that nickel has higher concentration in dendritic arms (dark zone), based on its more weight percentage, and for the light zone of interdendritic zone, copper was found to have higher concentration.

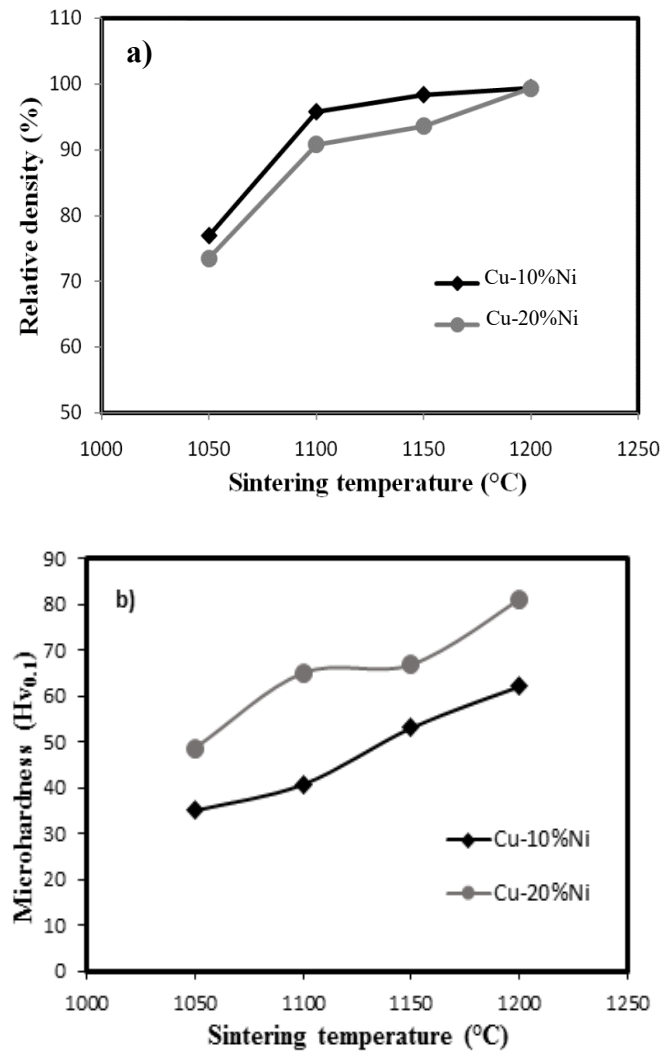


**Figure 6.** a) The relative density and b) the micro hardness vs. sintering temperature for the samples of Cu- 10% Ni and Cu-20% Ni

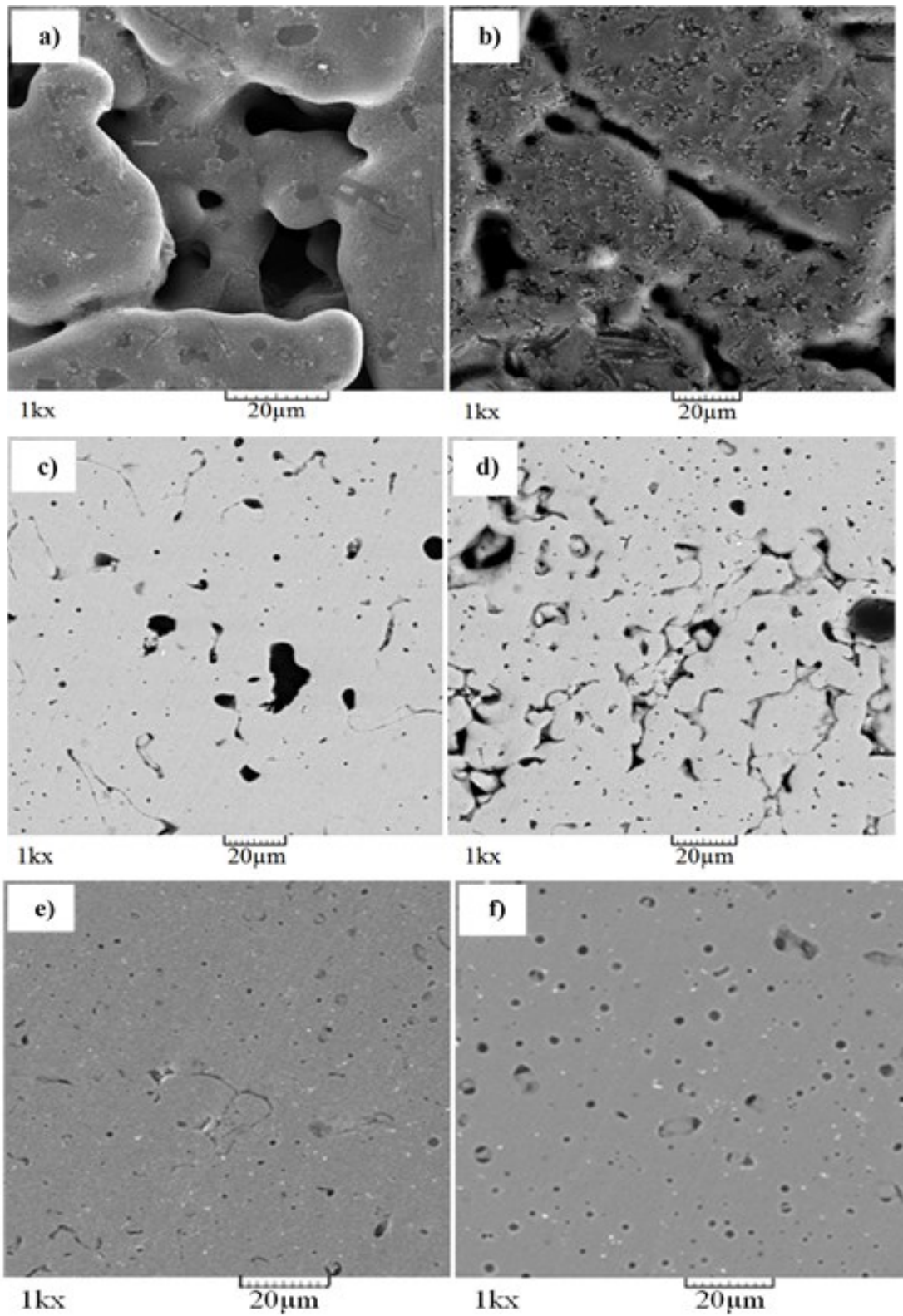


**Figure 7.** SEM micrographs of a) Cu-10 % Ni, b) Cu-20% Ni samples sintered at 1050 °C, c) Cu-10% Ni, d) Cu-20% Ni samples sintered at 1100 °C, and e) Cu-10% Ni, f) Cu-20% Ni samples sintered at 1150 °C

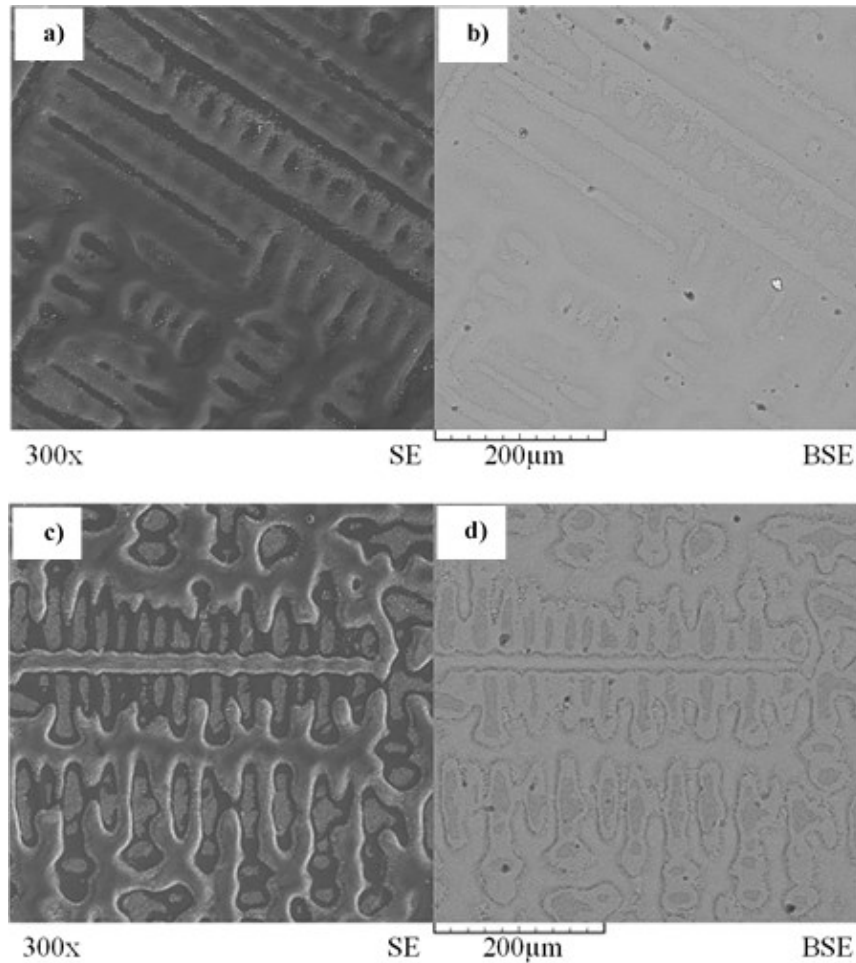


**Figure 8.** SEM (backscattered and secondary) micrographs of etched, sintered samples at 1200 °C a, b) Cu-10% Ni, c, d) Cu-20% Ni powders

The elemental map analysis of Ni and Cu for the sample of Cu-10% Ni that is illustrated in [Figure 9b](#) and [Figure 9c](#) showed more concentrated distribution of Cu in interdendritic area (light zone,) while the dendrites (dark zone) had higher Ni concentration. As the starting composite powder of Cu-Ni, resulted from chemical precipitation, are normally uniformly elemental distributed, such segregation was the result of liquid state sintering.

Nucleation and growth are the two major mechanisms that lead to the final structure of the solidifying metal. The origin of dendritic growth in solid solution is the rejection of the

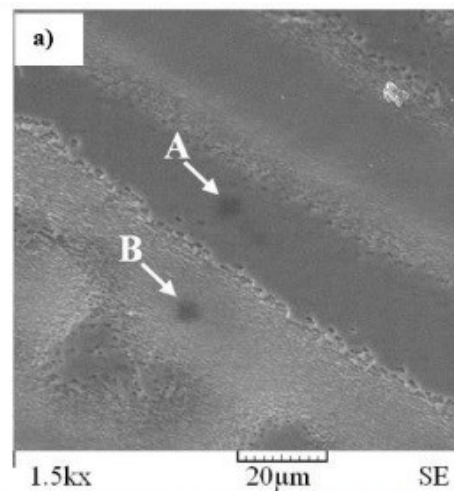
solute element by growing solid (when partition coefficient,  $k = \frac{C_s}{C_l}$ , is less than 1,

where  $C_s$  and  $C_l$  are partition coefficient, solute concentration in solid and liquid phases), termed as micro-scale segregation, which is a common phenomenon in alloys solidification [29–33]. Dendrites formation is caused through the diminished stability associated with the constitutional gradient in the melt phase ahead of the tip, called constitutional undercooling. As  $K$  is calculated to 1.52 for Cu-Ni liquidus line in the range of 10-20% Ni, the microsegregation of solute (Ni) was towards solid arms.

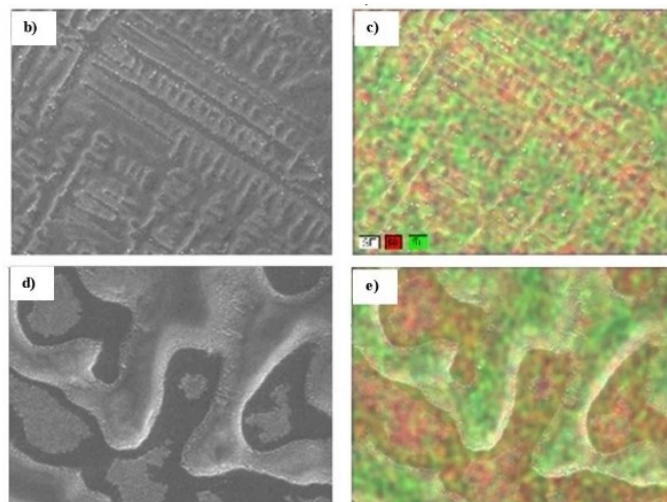
Microsegregation during solidification pushes Cu and hence leaves liquid area behind with lower melting point [32]. The average thickness of primary arms of dendrites for samples of 10% and 20% Ni sintered at 1200 °C were found to be 17.3 and 20.1  $\mu\text{m}$ , respectively. The bolder dendritic structure in the sample with higher Ni % (Figure 9) can be stemmed from the promoted segregation during solidification due to higher Ni content for dendrite formation.

Figure 9d and Figure 9e shows elemental map analysis of the sample with higher Ni (Cu-20% Ni), sintered at 1200 °C through liquid

state sintering. In this figure, dendritic branch has been shown in closer view and dispersion of copper and nickel can be observed clearly. This analysis confirmed more Ni concentration in dendritic areas which are depicted with green points in Figure 9e, while the most concentration of Cu, with red points, are located in the interdendritic regions. This is the same as detected for the sample of 10% Ni. The line analysis, which is shown in Figure 10, confirms above mentioned observations. As seen, by increasing the intensity of copper peaks, nickel intensity is decreased and inverse.



**Figure 9.** a) SEM image of sintered Cu-10% Ni sample at 1200 °C, b, c) map analysis of Cu-10% Ni, d, e) Cu-20% Ni samples, sintered at 1200 °C



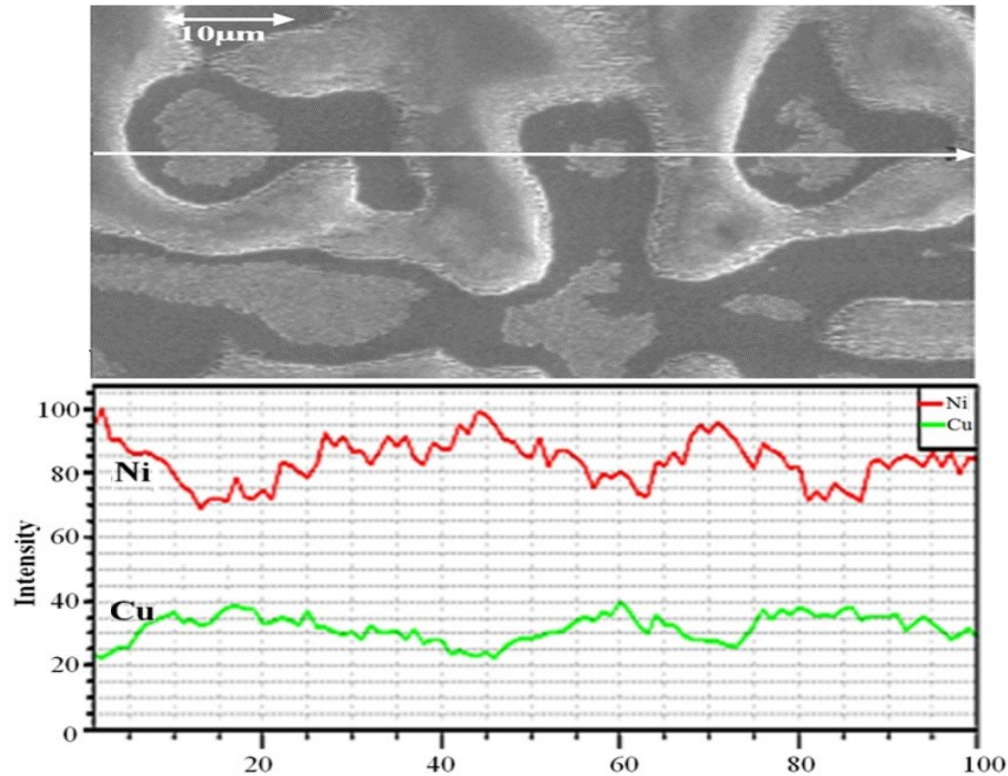


**Figure 10.** Linear analysis of sintered sample of Cu-10% Ni at 1200 °C

Referring to the literature, there are various studies on the sintering of Cu-Ni containing compositions, because this binary combination has gained interests for good properties of corrosion resistance, heat conduction, strength and also memory shaping [34–39]. Table 2 shows some details of previous works and current research for comparison. As seen, in addition to different mechanisms of sintering, the various starting combinations could affect the mechanical behavior such as hardness, either micro or macro; this makes it difficult to assess the individual effect of chemical precipitation method which was employed in the current study to synthesize nano-sized composite powder of Cu-Ni, on the mechanical properties of final bulk. However, Cu with the lowest melting temperature, in all works, has involved in liquid phase sintering. Comparing the relevant density of the products could be informative. As seen in this table, the relevant

density of the current work (99.45 and 99.4 g/m<sup>3</sup> for 10% Ni and 20% Ni respectively) is more than the other works, except for the researches benefiting sintering process assisted with hot forging in which a dense structure would be expected, although no value for density is reported [35, 40]. Nano scaled particles with uniformity in elemental distribution could be a promising factor that has a significant role on modifying the densification, in addition to its contribution on strengthening the material due to Hall-Petch equation.

### Conclusions

In the present study, nanostructured Cu-10 and 20 wt.% Ni powders were prepared by chemical precipitation route from copper and nickel sulfate salts as raw materials. Then, the initial precipitates were calcined in air, and was consequently reduced in hydrogen. The

**Table 2.** Hardness and density of sintered powders in literature and current study

	Particles Characteristics ( $\mu\text{m}$ )	Sintering Condition	Micro Hardness	Macro-Hardness	Density ( $\text{g}/\text{cm}^3$ )	Relative Density (%)
Cu-7.0Ni-1.75Si-0.5Cr [40]	25	Hot Pressed and Sintered 1000 °C+Hot Forged 850 °C	126 Hv	-	Not reported	-
Fe-Cu-30%Ni [34]	3	Pressed at 700 MPa 1150 °C for 30 min	-	57 RCA	7.12	90.58
W-10%Ni-10%Cu [35]	Nano size	Selective Laser Melting (SLM): 12 J/m <sup>3</sup> of energy density	380 Hv <sub>0.1</sub>	-	9.2	53.40
TiNi-10% Cu [36]	40+6.3	1125 °C for 5 h	-	-	Porous structure	Porous structure
Ti30Ni20Cu [37]		1100 °C for 3 h	-	-	Porous structure	Porous structure
Cu- 7Ni-1.7Si-0.4Cr - 0.6Al <sub>2</sub> O <sub>3</sub> [38]	Nano size	Sintered 1000 °C+Hot Forged 850 °C	187	-	Not reported	-
Cu-10%Ni (current Study)	Nano size	1200 °C	-	-	8.954	99.45
Cu-20%Ni (current Study)	Nano size	1200 °C	-	-	8.95	99.40

reduced products were finally pressed and sintered at different sintering temperatures. The effect of sintering temperature and nickel content on microstructure, relative density and hardness was investigated. The following results were obtained:

1. A compound powder of Cu<sub>4</sub>SO<sub>4</sub>(OH)<sub>6</sub>, Ni(OH)<sub>2</sub> and NiOOH were obtained through chemical precipitation. The following calcination and reduction produced CuO-NiO and Cu-Ni composite powder, respectively.
2. The products of precipitation, calcination and reduction were found to have nano-sized crystallites; under 35 nm.
3. It was found that increasing the temperature of sintering and decreasing nickel content

increased the relative density. The densification was significantly increased above the melting point of copper. Maximum value of the relative density was observed for Cu-10% Ni sample sintered at 1200 °C.

4. Sintering temperature had constructive effect on hardness of products for both 10 and 20% Ni.


5. Higher Ni in the sintered samples resulted in better hardness. The maximum hardness was found for Cu-20% Ni which was sintered at 1200 °C.

#### Disclosure Statement

No potential conflict of interest was reported by the authors.



## Orcid

Hurieh Mohammadzadeh 

<https://orcid.org/https://orcid.org/00>

## References

- [1]. Akhtar S., Saad M., Misbah M.R., Sati M.C. *Mater. Today Proc.*, 2018, **5**:18649
- [2]. Bains P.S., Sidhu S.S., Payal H.S. *Mater. Manuf. Process.*, 2016, **31**:553
- [3]. Akbarpour M.R., Alipour S., Farvizi M., Kim H.S. *Arch. Civ. Mech. Eng.* 2019, **19**:694
- [4]. Bader A., Elmajbry A., boriki Z.A., Ahmida A. *Prog. Chem. Biochem. Res.* 2020, **3**:1
- [5]. Songping W. *Microelectronics J.* 2007, **38**:41
- [6]. Ma X., Qi K., Wei S., Zhang L., Cui X. *J. Alloys Compd.* 2019, **770**:236
- [7]. Zad Z.R., Davarani S.SH., Taheri A., Bide Y. *J. Mol. Liq.* 2018, **253**:233
- [8]. Huang Y.W., Chao T.Y., Chen C.C., Cheng Y.T. *Appl. Phys. Lett.*, 2007, **90**:2005
- [9]. Chen T., Sun Y., Guo M., Zhang M. *J. Alloys Compd.*, 2018, **766**:229
- [10]. Gu D., Shen Y., Lu Z. ] *Mater. Des.*, 2009, **30**:2099
- [11]. Liu K., Wang Z., Yin Z., Cao L., Yuan J. *Ceram. Int.*, 2018, **44**:18711
- [12]. Anijdan S.H.M., Sabzi M., Zadeh M.R., Farzam M. *Tribol. Int.*, 2018, **127**:108
- [13]. Jena P.K., Brocchi E.A., Motta M.S. *Metall. Mater. Trans. B.*, 2004, **35**:1107
- [14]. Lakma A., Pradhan R.N., Hossain S.M., Van Leusen J., Kögerler P., Singh A.K. *Inorganica Chim. Acta.*, 2019, **486**:88
- [15]. Ahangarkani M. *Mater. Lett.*, 2020, **271**:127
- [16]. Yoshida M., Hasegawa A., Obata S., Sakurada O. *Mater. Today Proc.*, 2019, **16**:226
- [17]. Vilminot S., Richard-Plouet M., André G., Swierczynski D., Bourée-Vignerion F., Kurmoo M. *J. Chem. Soc. Dalton Trans.*, 2005, **6**:1455
- [18]. Chen H.C., Qin Y., Cao H., Song X., Huang C., Feng H., Zhao X.S. *Energy Storage Mater.*, 2019, **17**:194
- [19]. Schneiderová B., Demel J., Zhigunov A., Bohuslav J., Tarábková H., Janda P., Lang K. *J. Colloid Interface Sci.*, 2017, **499**:138
- [20]. Novikova A.A., Moiseeva D.Y., Karyukov E.V., Kalinichenko A.A. *Mater. Lett.*, 2016, **167**:165
- [21]. Mohammadzadeh H., Rezaie H., Samim H., Barati M., Razavizadeh H. *Mater. Chem. Phys.*, 2015, **149**:145
- [22]. Zhu W., Wang L., Zhao R., Ren J., Lu G., Wang Y. *Nanoscale.*, 2011, **3**:2862
- [23]. Choudhury P.K., Banerjee S., Ramaprabhu S., Ramesh K.P., Menon R. V. *J. Nanosci. Nanotechnol.* 2013, **13**:8162
- [24]. Azzerboni M.G.B., Asti G., Pareti L. *Magnetic nanostructures in modern technology: Spintronics, Magnetic MEMS and Recording*, Springer:New York, 2007; P62
- [25]. Oh M.C., Ahn B. *Trans. Nonferrous Met. Soc. China.*, 2014, **24**:53
- [26]. Taha M.A., Nassar A.H., Zawrah M.F. *Ceram.*, 2017, **43**:3576
- [27]. Guo Y., Jia L., Kong B., Zhang S., Sha J., Zhang H. *J. Alloys Compd.*, 2017, **696**:516
- [28]. Tongsrir R., Tosangthum N., Yotkaew T., Muthitamongkol P., Sri-On A., Patakham U. *Mater. Charact.*, 2016, **113**:52
- [29]. Sethi G., Park S.J., Johnson J.L., German R.M. *Int. J. Refract. Met. Hard Mater.*, 2009, **27**:688
- [30]. Hao H., Ye S., Yu K., Chen P., Gu R., Yu P. The role of alloying elements on the sintering of Cu, *J. Alloys Compd.* 2016, **684**:91
- [31]. Xu X.L., Zhao Y.H., Hou H. *J. Alloys Compd.*, 2019, **733**:1131
- [32]. Dündar S. *Turkish J. Eng. Environ. Sci.*, 2004, **28**:129
- [33]. Song A.J., Ma M.Z., Zhou R.Z., Wang L., Zhang W.G., Tan C.L., Liu R.P. *Mater. Sci. Eng. A.*, 2012, **538**:219

- [34]. Amador D.R., Torralba J.M. *J. Mater. Process. Technol.*, 2003, **70**:9
- [35]. Wang M., Li R., Yuan T., Chen C., Zhang M., Weng Q., Yuan J. *Int. J. Refract. Met. Hard Mater.*, 2018, **463**:250
- [36]. Zheng H.X., Mentz J., Bram M., Buchkremer H.P., Stöver D. *J. Alloys Compd.*, 2008, **23**:2029
- [37]. Jiang H.J., Ke C.B., Cao S.S., Ma X., Zhang X.P. *Trans. Nonferrous Met. Soc. China*, 2013, **728**:1157
- [38]. Sen Wang H., Chen H.G., Hsu C.E., Wu C.Y. *J. Alloys Compd.*, 2017, **48**:97
- [39]. Wang H., Zeng M., Liu J., Lu Z., Shi Z., Ouyang L., Zhu M. *Int. J. Refract. Met. H.*, 2015, **143**:781
- [40]. Sen Wang H., Chen H.G., Gu J.W., Hsu C.E., Wu C.Y. *J. Alloys Compd.*, 2015, **633**:59

**How to cite this manuscript:** Hurieh Mohammadzadeh\*, Roya Roohibakhsh, HamidReza Rezaie. An investigation on sintering behavior of nanostructured Cu-10, 20 wt. % Ni alloy powders. *Asian Journal of Nanoscience and Materials*, 4(2) 2021, 95-112. DOI: 10.26655/AJNANOMAT.2021.2.1